- 16 Beth Israel Deaconess Medical Center
- 17 330 Brookline Avenue - YA309

*Corresponding Author

JCM Accepted Manuscript Posted Online 29 November 2017

Copyright © 2017 American Society for Microbiology. All Rights Reserved.

Running Title: Gram stain interpretation with deep learning

^bHarvard Medical School, Boston, MA, USA

†These authors contributed equally to this work

Kenneth P. Smith†^{a,b}, Anthony D. Kang†^{a,b,c}, and James E. Kirby^{a,b#}

^aDepartment of Pathology, Beth Israel Deaconess Medical Center, Boston, MA

^cUnited States Army Medical Department Center and School, Fort Sam Houston, TX.

J. Clin. Microbiol. doi:10.1128/JCM.01521-17

Network

1

2

3

4

5

6

7

8

9

10

11

12

- 18 Boston, MA 02215
- 19 jekirby@bidmc.harvard.edu
- 20 Phone: 617-667-3648
- 21 Fax: 617-667-4533

22

23 Keywords: Gram stain, blood culture, machine learning, deep learning, automated microscopy

Automated Interpretation of Blood Culture Gram Stains using a Deep Convolutional Neural

Abstract

24

25

26

27

28

29

30

31

32

33

34

35

36

37

38

39

40

41

42

43

44

45

46

Microscopic interpretation of stained smears is one of the most operator-dependent and time intensive activities in the clinical microbiology laboratory. Here, we investigated application of an automated image acquisition and convolutional neural network (CNN)-based approach for automated Gram stain classification. Using an automated microscopy platform, uncoverslipped slides were scanned with a 40x dry objective, generating images of sufficient resolution for interpretation. We collected 25,488 images from positive blood culture Gram stains prepared during routine clinical workup. These images were used to generate 100,213 crops containing Gram-positive cocci in clusters, Gram-positive cocci in chains/pairs, Gram-negative rods, or background (no cells). These categories were targeted for proof-of-concept development as they are associated with the majority of bloodstream infections. Our CNN model achieved classification accuracy of 94.9% on a test set of image crops. Receiver operating characteristic curve (ROC) analysis indicated a robust ability to differentiate between categories with area under the curve >0.98 for each. After training and validation, we applied the classification algorithm to new images collected from 189 whole slides without human intervention. Sensitivity/specificity was 98.4/75.0% for Gram-positive cocci in chains/pairs; 93.2/97.2% for Gram-positive cocci in clusters; and 96.3/98.1% for Gram-negative rods. Taken together, our data support proof-of-concept for a fully automated classification methodology for blood-culture Gram-stains. Importantly, the algorithm was highly adept at identifying image crops with organisms and could be used to present prescreened, classified crops to technologists to accelerate smear review. This concept could potentially be extended to all Gram stain interpretive activities in the clinical laboratory.

Introduction

47

48

49

50

51

52

53

54

55

56

57

58

59

60

61

62

63

64

65

66

67

68

69

Bloodstream infections (BSI) are rapidly progressive infections with mortality rates up to nearly 40% (1, 2). Each day delay in institution of active antimicrobial therapy is associated with up to a ~10% increase in mortality (3, 4). Due to relatively low bacterial burden (<10 CFU mL ¹)(5), patient blood is pre-incubated in broth culture to detect presence of bacteria, typically by semi-continuous measurement of CO₂ production or pH with an automated blood culture instrument. If organism growth is detected, an aliquot of broth (now containing >10⁶ CFU mL⁻¹) is removed for Gram stain smear and subculture. The Gram stain provides the first critical piece of information that allows a clinician to tailor appropriate therapy and optimize outcome (6).

Despite recent advances in automation in other stages of the BSI diagnosis process (automated blood culture incubators and Gram staining systems) (7), Gram stain interpretation remains labor and time intensive, and highly operator-dependent. With consolidation of hospital systems, increasing workloads, and potential unavailability of highly trained microbiologists on site (8), automated image collection paired with computational interpretation of Gram stains to augment and complement manual testing would provide benefit. However, there has been a dearth of scientific exploration in this area, and several technical difficulties need to be overcome.

Practically, automated Gram stain interpretation requires both automated slide imaging and automated image analysis. Although automated slide scanners and microscopes are being used in anatomic pathology, for example, telepathology (9), their application in clinical microbiology has been limited based on several technical challenges. First, Gram stained slides are typically read using 100X objectives, greatly complicating image acquisition due to the need for addition of oil during scanning. Second, microbiology smear material can adequately be

71

72

73

74

75

76

77

78

79

80

81

82

83

84

85

86

87

88

89

90

91

92

imaged only in a very narrow field of focus, a challenge for existing slide scanners. Third, Gram stained slides exhibit ubiquitous and highly variable background staining. This background may cause autofocus algorithms to target areas that are either devoid of bacteria or miss the appropriate focal plane entirely. Image analysis to identify Gram stain characteristics presents separate hurdles. Importantly, background and staining artifacts, both fairly ubiquitous, often mimics the shape and color of bacterial cells. Therefore, algorithms relying on color intensity thresholding and shape detection will provide suboptimal accuracy.

Here, we provide proof-of-concept for automated, deep learning-based Gram stain analysis. The major conceptual and technical innovations were twofold. First, we developed an imaging protocol using an automated slide imaging platform equipped with a 40X air objective to collect highly resolved data from Gram-stained blood culture slides. Second, image data were used to train a convolutional neural network (CNN)-based model to recognize morphologies representing the most common causative agents of BSI: Gram-negative rods, Gram-positive cocci in clusters, and Gram-positive cocci in pairs or chains (1). CNNs are modeled based on the organization of neurons within the mammalian visual cortex, and were applied here based on their ability to excel in image recognition tasks without requiring time-intensive selective feature extraction by humans (10). Our trained model was subsequently evaluated for accuracy in comparison to manual classification.

Results

Slide collection and manual classification. Blood culture Gram stain slides prepared manually during the course of normal laboratory operation were used for analysis. Slides were selected based on the presence of any of the three most common morphotypes observed in

94

95

96

97

98

99

100

101

102

103

104

105

106

107

bloodstream infection: Gram-positive cocci in clusters, Gram-positive cocci in pairs and chains, and Gram-negative rods. Less common morphotypes (e.g. Gram-positive rods or yeast) and polymicrobial infections were excluded. To capture real-world variability, slides were not prescreened for suitability for automated microscopy or deep learning, and had characteristic slideto-slide variability in staining intensity, staining artifacts, and sample distribution. We anticipated that inherent variability would pose a real-world challenge to slide classification models.

Automated image collection. CNN-based deep learning models require large datasets for training, typically at least on the order of thousands of images (and ideally at least an order of magnitude more). Therefore, an automated microscopy image acquisition strategy was used. We performed image acquisition on the MetaFer Slide Scanning and Imaging Platform (MetaSystems Group, Inc., Newton, MA) based on a robust Gram stain-compatible autofocus system, ability to sample multiple distributed positions on a slide to account for variations in specimen distribution, and automated slide loading capability to enable high throughput slide scanning.

Clinically, Gram stains are read under oil immersion. However, semi-continuous addition of oil during automated microscopy was undesirable. In preliminary experiments with uncoverslipped slides (data not shown), we determined that the 40x dry objective provided sufficient resolution for machine-learning applications based on our prior experience (11). Therefore, we selected use of the 40x air objective for image acquisition, thus avoiding the requirement for oil immersion and allowing us to capture a larger field of view in each image.

Deep convolutional neural network training. For CNN training, a total of 25,488 images were automatically collected from distributed locations on 180 slides. A representative

117

118

119

120

121

122

123

124

125

126

127

128

129

130

131

132

133

134

135

136

137

138

image is shown in Fig. 1. This image demonstrates features typical of blood culture Gram stain smears including: (A) intense background staining; (B) stain crystallization artifact; (C) diffuse background staining; (D) individually resolvable, high-contrast Gram-negative cells; and (E) individually resolvable, low-contrast Gram-negative cells. Of note, ubiquitous background material was often similar in color, intensity, and/or shape to bacterial cells.

Highly experienced medical technologists can readily differentiate bacteria from this background. However, it is prohibitively difficult to manually define computational rules for Gram-stain classification that would adequately distinguish signal from noise in highly variable Gram-stain preparations. Therefore, we chose instead to use a deep learning approach, more specifically, a CNN, for image analysis. CNNs do not interpret raw images directly. Rather, they consist of a number of layers, each of which convolutes regions of the image to detect specific features. During each step of the learning process, a subset of images is presented to the network, allowing function parameters to be changed such that the CNN identifies features important for classification based on optimization of output accuracy. The final model is defined by a set of weights and biases that control the flow of information through the network such that the most discriminatory features in the images are used for classification.

Downloaded from http://jcm.asm.org/ on July 18, 2018 by guest

Each CNN model has a unique architecture that differs in organization, function and number of convolutional layers (10). The model used in our analysis, Inception v3, has previously been shown to perform robustly on complex image classification tasks including accurate classification of 1,000 different objects (12). The Inception v3 model is composed of a series of small convolutional networks termed "inception modules" and was designed to be less computationally intensive than comparable networks (13). Nevertheless, it is still a highly complex model requiring weeks to train even with state-of-the-art computational infrastructure

140

141

142

143

144

145

146

147

148

149

150

151

152

153

154

155

156

157

158

159

160

161

(12). However, training the entire network is not always necessary. Many image classification tasks can be addressed using pre-computed parameters from a network trained to classify an unrelated image set, a method called transfer learning (14). To this end, we used an Inception v3 model previously trained to recognize 1,000 different image classes from the 2012 ImageNet Large Scale Visual Recognition Competition dataset (15), and re-trained the final layer to identify our Gram stain categories of interest.

From an image analysis perspective, blood culture Gram stains are mostly background. This excessive background increases the chance that a CNN will learn features during training that are unrelated to bacterial Gram-stain classification. This is termed overfitting and results in a model with high accuracy in classifying images on which it was trained (the training set), but poor accuracy when presented with an independent validation set. Therefore, we enriched the training data through use of selected image crops rather than whole slide images. A training crop selection tool was created using the Python programming language which allowed the trainer to select areas of an image containing bacteria with a single mouse click. This allowed us to train our model on regions of images containing bacteria without inclusion of excessive background.

Downloaded from http://jcm.asm.org/ on July 18, 2018 by guest

For model training (Fig. 2), we used our training crop selection tool to generate a total of 100,213 manually classified image crops from 180 slides. Training and validation accuracy were indistinguishable (Fig. 2A), implying robust ability of the model to evaluate data on which it had not previously been trained. It further confirmed success in minimizing overfitting. During training, predictions made by our model were compared to the observed data, and differences between these values were quantified using a metric called cross-entropy (16). In practice, low cross-entropy indicates that the model fits the observed data well. Cross entropy decreased during training and plateaued after 12,000 iterations (Fig. 2B). Additional training iterations

163

164

165

166

167

168

169

170

171

172

173

174

175

176

177

178

179

180

181

182

183

184

beyond what is shown in Fig. 2 did not reduce cross-entropy or therefore improve model accuracy.

Evaluation of model performance on a per-crop basis. Our CNN outputs relative probabilities that an image crop belongs to each of four categories of training data: specifically, Gram-positive cocci in chains/pairs, Gram-positive cocci in clusters, Gram-negative rods, and background (i.e., no bacteria) (17). Per convention (10), the class with the highest probability is assigned as the predicted class. Using this method, we tested our model using a test set of image crops not used during model training, and achieved a classification accuracy of 94.9%, providing an initial estimate of model performance. However, this metric may be impacted by the fact that the test set was not wholly independent of the training set, as it may still contain crops from the same slide or images used in developing the training and validation sets.

Therefore, to rigorously evaluate ability of our model to generalize to an entirely independent dataset, we evaluated performance on an evaluation set of 4,000 manually classified image crops (n = 1,000 crops per class) from 59 slides that were not a component of the training, validation, or test sets. Here, we achieved a similar overall 93.1% image crop classification accuracy. Importantly, the evaluation set also allowed us to calculate sensitivity and specificity on a per-category basis. Sensitivity/specificity was 96.6/99.4% for Gram-positive clusters, 97.7/99.0% for Gram-positive chains, 80.1/99.4% for Gram-negative rods, and 97.4/93.0% for background. Calculation of the area under the receiver operating characteristic (ROC) curve (AUC) for each category (Fig. 3) further indicated robust ability to differentiate between categories (AUC > 0.98 for all).

Downloaded from http://jcm.asm.org/ on July 18, 2018 by guest

Development of whole-slide classification algorithm. To this point, we performed classifications on manually selected cropped images based on category assignment using the

186

187

188

189

190

191

192

193

194

195

196

197

198

199

200

201

202

203

204

205

206

207

highest probability output from the classification. However, we hypothesized that it was not the optimal way to interpret our results for whole-slide classification. Specifically, a whole slide classification task differs from our evaluation experiments in that it would necessarily examine a much larger number of crops that were not preselected and only consist of background. Given that background may simulate bacterial cells (Fig. 1), we expected a greater likelihood of false positive calls.

To test this possibility during whole-slide classification, we decided to set a very stringent probability cutoff (0.99) for category calls to minimize false positives at the image crop level and maximize specificity at the whole slide level. Using this stringent cutoff, 65.6% of evaluated crops had a prediction with confidence of ≥ 0.99 , and 99.6% of these were correctly classified. Classification accuracy was 99.9% for Gram-positive clusters, 100% for Grampositive chains, and 97.4% for Gram-negative rods.

Downloaded from http://jcm.asm.org/ on July 18, 2018 by guest

To investigate how this stringent cutoff would impact false-positive rate on a per slide basis when applied to images cropped automatically, we collected 350 whole images containing no visible cells and which were not part of the training, validation, and evaluation datasets. Images were cropped into 192 non-overlapping crops (n = 67,200) using a custom Python script and evaluated using our trained model with the classification threshold described above. For each category, false positive rates were ≤0.006% on a per image crop basis. Based on an assumed normal distribution of false positives calls, we set a minimal threshold for slide classification of 6 positive crops per category in order to achieve a desired ≤ 0.1% false positive whole-slide classification rate.

Our whole-slide classification algorithm was then tested on 189 slides previously classified manually by a microbiologist and not a component of the training, validation, test, or

209

210

211

212

213

214

215

216

217

218

219

220

221

222

223

224

225

226

227

228

229

230

evaluation sets. Each of 54 images scanned per slide was divided into 192 non-overlapping 146 x 146 pixel crops and evaluated using the parameters described above for a total of 10,368 crops per slide. We first qualitatively evaluated performance on automated image crops. This was achieved by writing a Python program (called TA for technologist assist) that would output images corresponding to crop calls by the CNN allowing for specific review. Fig. 4 shows examples of correctly classified image crops corresponding to each of the four classification labels.

We then quantitatively evaluated our whole slide classification accuracy in comparison to manual classification by constructing a table that shows each slide's manual classification and corresponding automated prediction (Table 1). We found that bacteria were detected in 84.7% (n = 160) of slides by our automated algorithm. For those slides where bacteria were detected, we calculated classification accuracy, sensitivity, and specificity. Classification accuracy was 92.5% across all categories. Sensitivity was >97% for Gram-negative rods and Gram-positive clusters. Sensitivity was lower for Gram-positive chains, largely owing to misclassifications as Grampositive clusters across a relatively lower overall number of slides (n = 40). Further, manual inspection of Gram-positive chains misclassified as clusters revealed that these slides were somewhat ambiguous owing to substantial clumping of cells. Specificity for Gram-positive chains and Gram-negative rods was >96%. Specificity was slightly lower (93.2%) for Grampositive clusters, again owing to misclassification of Gram-positive chains as clusters. Despite qualitative difference in background staining, accuracy of slides from aerobic bottles (88.8%) or anaerobic bottles (92.9%) was not significantly different (Fisher's exact test, P > 0.05).

Downloaded from http://jcm.asm.org/ on July 18, 2018 by guest

Overall, the most common error was misclassification of slides as background, representing 70.7% (n= 29) of all misclassifications. On manual review of images from these

232

233

234

235

236

237

238

239

240

241

242

243

244

245

246

247

248

249

250

251

252

253

slides, we found that 44.8% (n = 13) had insufficient crops with bacteria to make a positive call based on our pre-established thresholds. We found an additional 48.3% (n = 14) had organisms that were either out of focus or very low contrast, and of these, the majority (78.6%, n = 11) contained Gram-negative organisms, as expected based on superficial similarity to background material. The remaining 6.9% (n = 2) of slides contained highly elongated Gram-negative rods or minute Gram-negative coccobacilli. Neither morphology was a component of our training set. Gram stain category miscalls (n = 5) other than conflation of Gram-positive cocci in chains and Gram-positive cocci in clusters, were related to a combination of poor representation of the causal organism in crops and excessive background artifact.

Discussion

The Gram stain smear provides the first microbiological data to guide treatment for BSI. Notably, earlier results are correlated with positive patient outcome (6). However, interpretation of Gram stains is time intensive and strongly operator dependent, requiring a skilled technologist for interpretation. Concerningly, the most recent survey from the American Society for Clinical Pathology indicates that, as of 2014, trained microbiology technologist jobs in the United States have a vacancy rate of ~9%, and nearly 20% of technologists plan to retire in the next 5 years (8). This finding highlights the need for development of solutions to make the current work force more efficient. However, there has been relatively little progress in automation of tests requiring subjective interpretation such as the Gram stain.

Downloaded from http://jcm.asm.org/ on July 18, 2018 by guest

Lack of progress in this area is related to technical issues with automated microscopy and need for imaging interpretation algorithms that are robust to identifying rare organisms in the presence of variable background. Here, we demonstrated that the MetaFer Slide Scanning and

255

256

257

258

259

260

261

262

263

264

265

266

267

268

269

270

271

272

273

274

275

276

Imaging Platform provides a robust automated image acquisition system, capable of providing sufficient resolution for Gram stain analysis using a 40X dry objective. For such analysis, we chose to use a CNN based on its ability to excel in image analysis tasks with minimal human intervention. A summary of workflow for implementation, testing, and validation of our platform is provided in Fig. 5.

This work adds to the examples of successful CNN use in several areas of image-based diagnostics. These include detection of skin cancer (18); interpretation of echocardiograms (19); and detection of metastatic cancer in lymph nodes (20) in which combined contributions of pathologists and CNN increased sensitivity for diagnosis (21). A CNN has also previously been used by our group for early prediction of antibiotic minimal inhibitory concentrations in microscopy-based microdilution assays (11).

Importantly, CNNs improve in performance as more image data is added to the training set. Unlike other machine learning models, however, training on more data neither increases the size of a CNN model, nor the complexity of model implementation. Nevertheless, training of an entire CNN model requires substantial computational infrastructure. Here, we took advantage of an existing trained CNN and re-trained its final layers, a method called transfer learning (14, 18). In this way, we were able to train and implement our model using a standard office computer containing an Intel Core i7 CPU, 32GB RAM with no GPU (graphics processing unit, the computational workhorse for image analysis).

Downloaded from http://jcm.asm.org/ on July 18, 2018 by guest

Not surprisingly, implementation of the trained CNN for whole slide analysis using this computer infrastructure was relatively slow. We therefore piloted whole slide classification using a system containing an Nvidia GTX 1070 GPU. Though still underpowered compared to other currently available GPUs, it improved whole-slide classification time by a factor of 6, resulting

278

279

280

281

282

283

284

285

286

287

288

289

290

291

292

293

294

295

296

297

298

299

in a classification time of ~9 minutes. The best available GPUs are markedly more powerful than the GTX 1070 and are expected to provide even better performance (<5 minutes per slide), not even considering the ability of CNN algorithms to distribute computations across multiple GPUs.

Overall, we found that our trained model performed well on whole-slide image classification. Where cells were detected, we achieved overall classification accuracy of 92.5% and specificity of >93% for all classification labels with no human intervention. The most common classification error from our model was misclassification of slides containing rare bacteria as background, representing the majority (70.7%) of all classification errors. In practice, these misclassifications would be flagged for direct technologist review, making these lowconsequence errors. We also note that our sensitivity/specificity in whole slide image classification accuracy was modestly lower than on a per-image-crop basis. This is likely due in part to inclusion of slides with very few bacteria and therefore higher propensity for falsepositives. Optimization of data collection or slide preparation would likely bring our whole-slide accuracy close to that of per-image-crop accuracy.

Downloaded from http://jcm.asm.org/ on July 18, 2018 by guest

Our study had several limitations. As a proof-of-principle examination, we included only the most common BSI pathogens and omitted several important, but less common bacterial morphologies, largely due to limitation in availability of training data. However, given an appropriate amount of training data, these could easily be incorporated into the Inception v3 model, which can distinguish 1000 different categories and will be a future goal. Similarly, discrimination of polymicrobial infections could be incorporated by inclusion of "mixed" categories into our algorithm.

We also recognize that there are several steps that could be taken to improve classification. Foremost, the number of slides (and therefore image crops) used for training is

301

302

303

304

305

306

307

308

309

310

311

312

313

314

315

316

317

318

319

320

321

322

relatively modest and could be increased to improve CNN accuracy. In addition, our whole slide scanning protocol was based on selecting pre-defined positions for imaging that were invariant between slides. This contributed to inadequate sampling in a significant subset of slides, which we believe was the greatest contributor to reduction in model accuracy. This hypothesis is supported by the observation that misclassified whole slide calls were typically from slides with very few bacteria or poor sample spread. Notably, to address this issue, it is possible with the existing microscope platform to perform an automated rapid scan for areas of appropriate staining intensity and thereby pre-select regions of the slide that are more likely to have sufficient Gram stained sample for image acquisition.

Gram stain smear preparation is also expected to have a significant impact on automated slide imaging. Here, we used slides prepared by technologists during the course of normal laboratory operation. Slides exhibited a high degree of variability in smear area, thickness, location, and staining intensity. We anticipate that standardization of these variables will improve ability of an automated microscope to consistently sample microscopic fields with evaluable organisms. Further, use of an automated Gram stain device for staining would also increase reproducibility of staining characteristics and further enhance accuracy. We plan to investigate all of these areas in the future.

Downloaded from http://jcm.asm.org/ on July 18, 2018 by guest

We envision a potential role of our technology in augmenting technologist classification. Given that manual interpretation of blood culture Gram stains by trained technologists are very accurate (22-24), our model could be used to enhance productivity by selectively presenting crops containing bacteria to local or remote technologists. This would increase efficiency of classification by sparing the operator the need to manually locate fields of interest among a preponderance of background. This would also conceivably reduce technologist read time from

minutes to seconds. Upon further development and intensive algorithm training, the platform could potentially also be used as a fully automated classification platform with no human intervention.

In the era of laboratory consolidation and limitations in the number of skilled technologists (8), we believe our system could provide enhanced opportunities for rapid Gram stain classification at the site of care or during understaffed shifts in conjunction with later analysis at a central laboratory or day shifts. We further envision extension of CNN analysis to other smear-based microbiological diagnostics in the parasitology, mycobacteriology, and mycology laboratories. We believe that this technology could form the basis of a future diagnostic platform that provides automated smear classification results and augments capabilities of clinical laboratories.

Downloaded from http://jcm.asm.org/ on July 18, 2018 by guest

334

335

336

337

338

339

340

341

342

343

344

345

323

324

325

326

327

328

329

330

331

332

333

Materials and Methods

Slide collection and manual slide classification. A total of 468 de-identified Gramstained slides from positive blood cultures were collected from the clinical microbiology laboratory at Beth Israel Deaconess Medical center between April and July, 2017 under an IRBapproved protocol. Slides were prepared during the course of normal clinical workup. No preselection of organism identity, organism abundance, or staining quality was performed prior to collection. Positive blood culture broth Gram stains included those prepared from both non-lytic, BD BACTEC Standard Aerobic (n = 232) and lytic, BD BACTEC Lytic Anaerobic Medium (n = 196) (BD, Sparks, MD).

All slides were imaged without coverslips using a MetaFer Slide Scanning and Imaging platform (MetaSystems Group, Inc., Newton, MA) with a 140-slide capacity automated slide

347

348

349

350

351

352

353

354

355

356

357

358

359

360

361

362

363

364

365

366

367

368

loader equipped with a 40x magnification Plan-Neofluar objective (0.75 Numerical Aperture, Zeiss, Oberkochen, Germany). For each slide, 54 images were collected from defined positions spanning the entirety of the slide. The first 279 slides collected were used in training, validation, and evaluation of our deep-learning model. The remaining 189 slides were classified manually as Gram-negative rods, Gram-positive chains/pairs or Gram-positive clusters using a Nikon Labophot 2 (Nikon Inc., Tokyo, Japan) microscope equipped with a 100x oil objective. Results were recorded for later use in evaluation of our whole-slide classification algorithm.

Training a Deep Convolutional Neural Network. A training dataset consisting of 146 x 146 pixel image crops was generated manually with the assistance of a custom Python script. The script allowed crop selection, classification, and file archiving with a single mouse click allowing large numbers of annotated crops to be saved in a short period of time in a manner directly accessible to the deep learning training program. Each crop was assigned to one of four classifications: Gram-positive cocci in pairs or chains, Gram-positive cocci in clusters, Gramnegative rods, or background (no cells). Prior to training, the dataset was randomly divided into three subsets: 70% of image crops were used to train the model, 10% were reserved for hold-out validation during model training, and 20% were reserved for testing to evaluate model performance after completion of training. We used a transfer learning technique based on the Inception v3 convolutional neural network (CNN) architecture pre-trained on the ImageNet Large Scale Visual Recognition Competition (ILSVRC) 2012 image database (12). We used the Python language (version 3.5) and the TensorFlow library (25)(version 1.0.1) to retrain the final layer of the model using a custom graphical user interface (GUI) controlling a modified script ("retrain.py") found in the TensorFlow GitHub repository (25, 26). Training was performed using mini-batch gradient descent (batch size 200) with Nesterov momentum (momentum = 0.9)

Downloaded from http://jcm.asm.org/ on July 18, 2018 by guest

370

371

372

373

374

375

376

377

378

379

380

381

382

383

384

385

386

387

388

389

390

391

(27) and cross-entropy as the loss function (16). The initial learning rate was 0.001 and decayed exponentially at a rate of 0.99 per epoch. The output layer was a 4-way softmax classification which assigned probabilities to each of the four categories described above.

Analysis of model performance on a per-crop basis. Using our trained CNN, we evaluated model performance on a per-image-crop basis using an evaluation set of 1,000 manually selected crops from each class (total crops = 4,000), all of which were independent of the training, validation, and testing datasets. For each category, true positives were defined as a crop correctly classified as the category of interest; false positives were defined as crops that were incorrectly classified as the category of interest; true negatives were defined as crops correctly classified as a category other than the category of interest; and false negatives were defined as crops incorrectly classified as a category other than the category of interest. Sensitivity and specificity were modeled as receiver operating characteristic (ROC) curves for each classification label by varying the softmax classification thresholds required for positivity. Sensitivity Specificity defined defined as True Positive+False Negative True Negative+False Positive. Area under the ROC curve (AUC) was calculated for each label using the trapezium rule as implemented in the scipy library (28). ROC curves were visualized using the matplotlib library (29).

Development of whole-slide classification algorithm. False positive rates for automatically cropped images containing only background were determined by analysis of 350 whole images from 40 different slides. Images contained no visible cells and were independent of the training, validation, testing, and evaluation datasets. Each image was automatically segmented into 192 non-overlapping crops of 146 x 146 pixels using a custom Python script (total crops = 67,200) and classified with our trained CNN using a stringent cutoff for positivity

393

394

395

396

397

398

399

400

401

402

403

404

405

406

407

408

409

410

411

412

413

414

(cutoff = 0.99). If no label achieved a probability greater than or equal to the cutoff, the associated crop was called background. False positive rates were recorded for each classification label.

Whole-slide classification. Using the automated imaging protocol outlined in the "Automated Image Collection" section, we evaluated whole slide classification accuracy using images collected from 189 slides which were previously manually classified (outlined in the "slide collection and manual slide classification" section). For each slide, a custom Python script was employed to automatically divide each image of the 54 images collected from predefined locations into 192 crops of 146 x 146 pixels. Each crop was evaluated by our trained deeplearning model and probabilities assigned to each category (Gram-negative rods, Gram-positive chains/pairs, Gram-positive clusters, or background) with a stringent cutoff for classification (cutoff = 0.99). If no label met the classification cutoff, the crop was classified as background.

After classification of all crops from a slide, the category corresponding to the greatest number of predicted crops was selected; however, only if the number of crops in the selected category exceeded the number of expected false positives (calculated in the "Determination of False Positive Rate" section). If none of the three label categories representing organisms were selected based on these criteria, the slide was classified as background. All results were recorded and used to construct a confusion matrix tabulation per convention in the deep learning field (30). Whole-slide sensitivity and specificity were defined and calculated as in the "Analysis of model performance on a per-crop basis" section. Classification accuracy for slides from aerobic or anaerobic bottles was compared using Fisher's exact test with significance defined as P < 0.05(JMP Pro version 13.0).

Downloaded from http://jcm.asm.org/ on July 18, 2018 by guest

416

417

418

419

420

421

422

423

424

425

426

427

428

429

430

431

432

433

434

Downloaded from http://jcm.asm.org/ on July 18, 2018 by guest

Acknowledgements We would like to thank Andreas Plesch, Ulrich Klingbeil, Bill Hanifin, (MetaSystems Group, Inc., Newton, MA) for providing use of the MetaFer Slide Scanning and Imaging Platform and Jenae Guinn (MetaSystems) for assistance in collection of image data. MetaSystems had no role in any other aspect of study design, data analysis or decision to publish. We thank Ramy Arnaout (Beth Israel Deaconess Medical Center, Boston, MA) for critical reading of the manuscript. **Funding Information**

This work was conducted with support from Harvard Catalyst | The Harvard Clinical and Translational Science Center (National Center for Research Resources and the National Center for Advancing Translational Sciences, National Institutes of Health Award UL1 TR001102) and financial contributions from Harvard University and its affiliated academic healthcare centers. Anthony Kang was supported by the Long Term Health Education and Training program from the United States Army as an American Society for Microbiology Committee on Postgraduate Educational Programs Fellow at Beth Israel Deaconess Medical Center. Kenneth Smith was supported by the National Institute of Allergy and Infectious Diseases of the National Institutes of Health under award number F32 AI124590. The content is solely the responsibility of the authors and does not necessarily represent the official views of the National Institutes of Health, United States Army, or Department of Defense.

References

435

- 436 1. Laupland KB. 2013. Incidence of bloodstream infection: a review of population-based
- 437 studies. Clin Microbiol Infect 19:492-500.
- 438 2. Wisplinghoff H, Bischoff T, Tallent SM, Seifert H, Wenzel RP, Edmond MB. 2004.
- 439 Nosocomial bloodstream infections in US hospitals: analysis of 24,179 cases from a
- 440 prospective nationwide surveillance study. Clin Infect Dis 39:309-17.
- 441 3. Schwaber MJ, Carmeli Y. 2007. Mortality and delay in effective therapy associated with
- 442 extended-spectrum beta-lactamase production in Enterobacteriaceae bacteraemia: a
- 443 systematic review and meta-analysis. J Antimicrob Chemother 60:913-20.
- Kang CI, Kim SH, Kim HB, Park SW, Choe YJ, Oh MD, Kim EC, Choe KW. 2003. 444 4.
- 445 Pseudomonas aeruginosa bacteremia: risk factors for mortality and influence of delayed
- 446 receipt of effective antimicrobial therapy on clinical outcome. Clin Infect Dis 37:745-51.
- 447 5. Wain J, Diep TS, Ho VA, Walsh AM, Nguyen TT, Parry CM, White NJ. 1998.
- 448 Quantitation of bacteria in blood of typhoid fever patients and relationship between
- 449 counts and clinical features, transmissibility, and antibiotic resistance. J Clin Microbiol
- 450 36:1683-7.
- 451 Barenfanger J, Graham DR, Kolluri L, Sangwan G, Lawhorn J, Drake CA, Verhulst SJ, 6.
- 452 Peterson R, Moja LB, Ertmoed MM, Moja AB, Shevlin DW, Vautrain R, Callahan CD.
- 453 2008. Decreased mortality associated with prompt Gram staining of blood cultures. Am J
- 454 Clin Pathol 130:870-6.
- 455 7. Bourbeau PP, Ledeboer NA. 2013. Automation in clinical microbiology. J Clin Microbiol
- 456 51:1658-65.

- 457 8. Garcia E, Ali AM, Soles RM, Lewis DG. 2015. The American Society for Clinical
- 458 Pathology's 2014 vacancy survey of medical laboratories in the United States. Am J Clin
- 459 Pathol 144:432-43.
- 460 Meyer J, Pare G. 2015. Telepathology Impacts and Implementation Challenges: A
- 461 Scoping Review. Arch Pathol Lab Med 139:1550-7.
- 462 10. LeCun Y, Bengio Y, Hinton G. 2015. Deep learning. Nature 521:436-44.
- 463 11. Smith KP, Richmond DL, Brennan-Krohn T, Elliott HL, Kirby JE. 2017. Development of
- 464 MAST: A Microscopy-Based Antimicrobial Susceptibility Testing Platform. SLAS
- 465 Technol doi:10.1177/2472630317727721:2472630317727721.
- Szegedy C, Vanhoucke V, Ioffe S, Shlens J, Wojna Z. Rethinking the Inception 466 12.
- 467 Architecture for Computer Vision. https://arxiv.org/abs/1512.00567. Accessed Sept. 12,
- 468 2017.
- Szegedy C, Wei L, Yangqing J, Sermanet P, Reed S, Anguelov D, Erhan D, Vanhoucke 469 13.
- 470 V, Rabinovich A. Going deeper with convolutions, p 1-9. In (ed),
- 471 14. Shin H-C, Roth HR, Gao M, Lu L, Xu Z, Nogues I, Yao J, Mollura D, Summers RM.
- 472 2016. Deep Convolutional Neural Networks for Computer-Aided Detection: CNN
- 473 Architectures, Dataset Characteristics and Transfer Learning. IEEE Transactions on
- 474 Medical Imaging 35:1285-1298.
- Russakovsky O, Deng J, Su H, Krause J, Satheesh S, Ma S, Huang Z, Karpathy A, 475 15.
- 476 Khosla A, Bernstein M, Berg AC, Fei-Fei L. 2015. ImageNet Large Scale Visual
- 477 Recognition Challenge. International Journal of Computer Vision 115:211-252.
- de Boer P-T, Kroese D, Reuven S, Rubinstein RY. 2005. A Tutorial on the Cross-478 16.
- 479 Entropy Method. Annals of Operations Research 134:19-67.

- 480 17. Bridle JS. 1989. Probabilistic Interpretation of Feedforward Classification Network
- 481 Outputs, with Relationships to Statistical Pattern Recognition. Neurocomputing
- 482 F68:227-236.
- 483 Esteva A, Kuprel B, Novoa RA, Ko J, Swetter SM, Blau HM, Thrun S. 2017. 18.
- 484 Dermatologist-level classification of skin cancer with deep neural networks. Nature
- 485 542:115-118.
- Madani A, Arnaout R, Mofrad M, Arnaout R. 2017. Fast and accurate classification of 486 19.
- 487 echocardiograms using deep learning.
- 488 https://arxiv.org/ftp/arxiv/papers/1706/1706.08658.pdf. Accessed Sept. 22, 2017.
- Litjens G, Sanchez CI, Timofeeva N, Hermsen M, Nagtegaal I, Kovacs I, Hulsbergen-van 489 20.
- 490 de Kaa C, Bult P, van Ginneken B, van der Laak J. 2016. Deep learning as a tool for
- 491 increased accuracy and efficiency of histopathological diagnosis. Sci Rep 6:26286.
- 492 21. Wang D, Khosla A, Gargeya R, Irshad H, Beck AH. 2016. Deep Learning for
- 493 Identifying Metastatic Breast Cancer. https://arxiv.org/abs/1606.05718. Accessed Sept.
- 494 12, 2017.
- 495 22. Samuel LP, Balada-Llasat JM, Harrington A, Cavagnolo R. 2016. Multicenter
- 496 Assessment of Gram Stain Error Rates. J Clin Microbiol 54:1442-7.
- 497 23. Sogaard M, Norgaard M, Schonheyder HC. 2007. First notification of positive blood
- 498 cultures and the high accuracy of the gram stain report. J Clin Microbiol 45:1113-7.
- 499 Rand KH, Tillan M. 2006. Errors in interpretation of Gram stains from positive blood 24.
- 500 cultures. Am J Clin Pathol 126:686-90.
- 501 25. TensorFlow: An open-source software library for Machine Anonymous. 2017.
- 502 Intelligence https://www.tensorflow.org/. Accessed Sept. 12, 2017.

503 26. Anonymous. 2017. TensorFlow GitHub Repository. 504 https://github.com/tensorflow/tensorflow. Accessed Sept. 12, 2017. 505 27. Nesterov Y. 1983. A method of solving a convex programming problem with 506 convergence rate O(1/sqr(k)). Soviet Mathematics Doklady 27:372-376. 507 28. Jones E, Oliphant E, Peterson P. 2001. SciPy: Open Source Scientific Tools for Python. 508 http://www.scipy.org/. Accessed Sept. 12, 2017. 509 29. Hunter JD. 2007. Matplotlib: A 2D graphics environment. Computing in Science and 510 Engineering 9:90-95. 511 30. Stehman SV. 1997. Selecting and interpreting measures of thematic classification 512 accuracy. Remote Sensing of Environment 62:77-89. 513

526

527

528

529

530

531

532

533

534

535

536

537

Figures Legends

516 517 Figure 1. Representative image collected using our automated imaging protocol. This image 518 shows several features characteristic of blood culture Gram stains including (A) area of intense 519 background staining, (B) artifact from stain crystallization, (C) diffuse background staining, and 520 individually resolved Gram-negative rods with (D) high and (E) low contrast compared to 521 background. 522 523 Figure 2. CNN Model Training Results. (A) Training and validation accuracy increased 524 exponentially, plateauing at ~95%. There was no observable difference in training and validation 525 accuracy, implying negligible overfitting during training. (B) Cross entropy is a metric used for

comparing model predictions to observed data. Lower cross entropy values indicate a better fit of the model to the data. During training, we observed that cross entropy decreased to a final value of ~0.1. Cross entropy plateaued at approximately 12,000 training iterations indicating that additional learning was not possible without increasing the number of input images, a goal of future work.

Figure 3. Receiver operating characteristic (ROC) curve. Curves were generated for each category by varying threshold for positivity. Area under the curve is indicated in parentheses.

Figure 4. Automatically classified crops. Each image represents a correctly classified crop that was automatically extracted from an image during whole slide classification. Rows of images represent (A) background, (B) Gram-positive chains/pairs, (C) Gram-positive clusters, or (D)

Gram-negative rods. One practical application of the platform would be to present such organism enriched images to a technologist to expedite smear review.

540

541

542

543

544

545

546

547

548

549

550

551

552

553

554

555

556

538

539

Figure 5. Summary of CNN training and evaluation. Prior to CNN training, we collected images using an automated microscopy protocol (image example shown in Fig. 1). For CNN training and preliminary testing, 100,213 image crops were manually selected, classified, and randomly partitioned into training, validation, and test sets. Sizes of boxes correlate to relative size of each data set. During iterative model training, accuracy was monitored using the training and validation sets (Fig 2.). After completion of training, model accuracy was initially assessed by quantification of accuracy on the test set (as discussed in text). However, the test set image crops came from the same slides as the training set. We therefore further assessed performance using a completely independent evaluation set to obtain a more reliable, real-world readout of image crop classification accuracy and to generate receiver operating characteristics (ROC) shown in Fig 3. Finally, we used a second independent dataset of automatically generated image crops from 189 slides to evaluate whole slide classification accuracy. Each whole slide classification was based on aggregate CNN categorizations of all image crops from a given slide (examples of such crops are shown Fig. 4). Accuracy was determined in comparison to manual slide interpretation (Table 1).

Downloaded from http://jcm.asm.org/ on July 18, 2018 by guest

Table 1. Confusion matrix of whole-slide classification results. 557

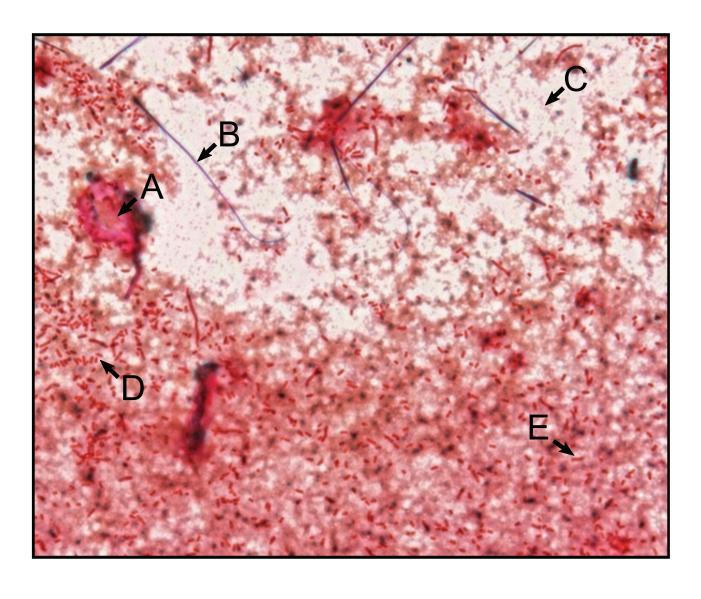
Predicted Classification (n)

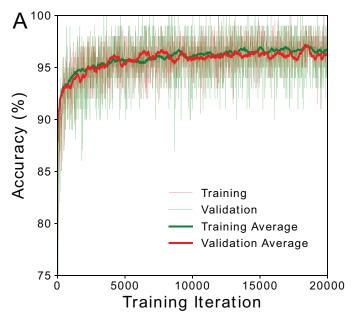
Human Classification	Gram-negative	Gram-positive pairs or chains	Gram-positive clusters	Background	Sensitivity % % (CI) ^a	Specificity % (CI) ^a
Gram-negative	51	1	0	17	98.1 (94.3-100)	96.3 (93.7-98.9)
Gram-positive pairs or chains	3	27	6	4	75.0 (60.9-89.0)	98.4 (90.8-100)
Gram-positive clusters	1	1	70	8	97.2 (93.4-100)	93.2 (89.7-96.6)

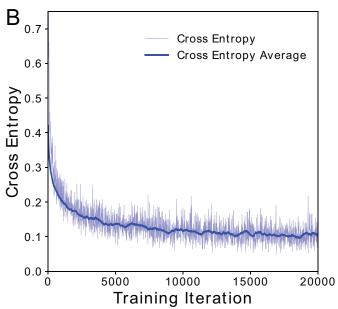
558

559 CI = 95% confidence interval

560 ^aBased on slides where bacteria were detected







Downloaded from http://jcm.asm.org/ on July 18, 2018 by guest



